International Immunopharmacology 75 (2019) 105794

Contents lists available at ScienceDirect

International Immunopharmacology

journal homepage: www.elsevier.com/locate/intimp

MiR-150 attenuates LPS-induced acute lung injury via targeting AKT3

Pibao Li[a,b], Yanfen Yao[b], Yuezhen Ma[b], Yanbin Chen[a,*]

[a] Department of Pulmonary and Critical Care Medicine, The First Affiliated Hospital of Soochow University, 899# Pinghai Road, Suzhou 215000, Jiangsu, China
[b] Department of Intensive Care Unit, Shandong Provincial Third Hospital, No.12, Central Wuying Hill Road, Jinan 250031, Shandong, China

ARTICLE INFO

Keywords:
miR-150
AKT3
LPS
ALI
ARDS

ABSTRACT

Acute lung injury (ALI) and its severe manifestation of acute respiratory distress syndrome (ARDS) in human lung are induced by inflammatory cytokines and endogenous factors such as miRNAs. However, the role of miR-150 in lipopolysaccharide (LPS)-induced ALI is not clear. Here, we found miR-150 expression was significantly reduced in the serum of patients with ARDS, and negatively associated with the disease severity and 28-day survival of ARDS. In vivo, miR-150 decreased total cell and neutrophil counts, and production of inflammatory cytokines interleukin-1β (IL-1β), interleukin-6 (IL-6) and tumor necrosis factor-α (TNF-α) as well as levels of total protein, albumin and IgM in the bronchoalveolar lavage (BAL) fluid in LPS-induced ALI mice. Meanwhile, miR-150 improved the 72 h survival rate of LPS-induced ALI mice. In-vitro assays demonstrated that miR-150 alleviated LPS-induced A549 cell apoptosis, autophagy, and release of inflammatory cytokines. Further, AKT3 was a direct target of miR-150. Silencing of AKT3 partially reversed LPS-induced A549 cell injury, and enhanced the protective effects of miR-150. In addition, miR-150 or si-AKT3 effectively inhibited the phosphorylation levels of c-Jun N-terminal kinase (JNK) and nuclear factor-κB (NF-κB) (p65 and IκBα). In conclusion, miR-150 alleviated LPS-induced acute lung injury via directly targeting AKT3 expression or regulating JNK and NF-κB pathways, which may be a promising therapeutic strategy to treat ALI/ARDS.

1. Introduction

ALI/ARDS, a common clinical syndrome, is characterized by excessive inflammatory reactions in lung tissues and loss of alveolar-capillary membrane integrity, resulting in accumulation of high-protein edema fluid in the lungs [1–3]. Till now, some novel therapeutic methods have improved the survival of patients with ARDS; however, the annual mortality for ALI/ARDS is still > 40%. Thus it is essential to investigate the molecular mechanisms of ALI/ARDS to design more effectively and usefully therapeutic targets.

MicroRNAs (miRNAs, miRs), a kind of small non-coding RNAs, play a vital role in the regulation of cell metabolism, viability, apoptosis, and inflammation [4,5]. MiRNAs have been identified as diagnostic biomarkers in the serum of some human diseases [6]. Current reports indicated that miR-150 plays a crucial role in modulating endothelial cell cycle and apoptosis, and maintaining internal homeostasis. MiR-150 has been demonstrated to be decreased in plasma of patients with sepsis [7]. In addition, down-regulated miR-150 expression in human serum is obviously associated with poor prognosis of patients with hepatic or renal dysfunction [8]. Therefore, emerging evidence indicated miR-150 may serve as a potentially diagnostic or prognostic biomarker in sepsis and organ injury.

To date, the expression and role of miR-150 in LPS-induced ALI are still unclear. Little is known about the suppression of inflammatory cytokines and relevant signaling pathways by miR-150. In this study, we aimed to investigate its molecular mechanisms underlying LPS-induced ALI.

2. Materials and methods

2.1. Participants

The human study was approved by the Ethics Committee of Shandong Provincial Third Hospital (SLSY-H-201801). The informed consent was obtained prior to experiment. 120 cases of patients with ARDS were enrolled and all the peripheral blood samples were drawn and collected. All patients in ARDS group met the ARDS Berlin definition of 2012. Firstly, patients had high risk factors for direct lung injury

Abbreviations: 3′-UTR, 3′-untranslated region; ALI, acute lung injury; ARDS, acute respiratory distress syndrome; BAL, bronchoalveolar lavage; IL-1β, interleukin-1β; IL-6, interleukin-6; JNK, c-Jun N-terminal kinase; LPS, lipopolysaccharides; miR-150, microRNA-150; miR-NC, negative control miRNA; NF-κB, nuclear factor-κB; TNF-α, tumor necrosis factor-α

* Corresponding author.
E-mail address: chenyanbinsoochow@163.com (Y. Chen).

https://doi.org/10.1016/j.intimp.2019.105794
Received 25 June 2019; Received in revised form 22 July 2019; Accepted 29 July 2019
Available online 06 August 2019

Table 1
The clinical characteristics of included subjects.

Indicators	Healthy control (n = 60)	ARDS (n = 120)
Age (years)	55.6 ± 14.2	55.9 ± 19.9
Gender (Male, %)	33 (66.0%)	85 (70.8%)
BMI (kg/m^2)	25.16 ± 4.41	24.22 ± 3.91
Cigarette smoking	31/60	91/120
Drink	44/60	104/120
Serum albumin level (g/dL)	3.1 ± 0.9	3.3 ± 0.8
FVC, % of prediction	86.7 ± 25.0	90.6 ± 17.9
FEV1, % of prediction	88.1 ± 24.7	90.4 ± 18.5
PaO2/FiO2		176.50 ± 13.76
APACHE II score		22.73 ± 3.48
SOFA score		11.19 ± 3.51
LIS score		2.79 ± 0.32
Causes of ARDS		
Postoperative		62
Lung contusion		19
Neurologic failure		17
Sepsis		12
Shock		8
Cardiovascular		2

APACHE II: acute physiologic and chronic health evaluation; ARDS: acute respiratory distress syndrome; BMI: body mass index; FEV1: forced expiratory volume in 1 s; FVC: forced vital capacity; LIS: lung injury score; SOFA: sequential organ failure assessment.

or indirect injury. Secondly, acute onset, heart failure, and fluid overload do not fully explain respiratory failure, and there is no high hydrostatic pulmonary edema. Thirdly, the specific detection data included hypoxemia: PaO2/FiO2 ≤ 300 mmHg in ALI and PaO2/FiO2 ≤ 200 mmHg in ARDS. Fourthly, Chest imaging changes, chest X-ray or CT scan images show infiltrated shadows in both lungs. Fifthly, pulmonary arterial wedge pressure ≤ 18 mmHg or left atrial hypertension was excluded. Clinical data of ARDS patients were collected from the medical record system of our hospital and summarized in Table 1. Healthy controls (n = 60) were recruited from among the Institute personnel, who were in excellent health during this study.

Table 2
Comparison of clinical characteristics of patients with ARDS according to survival.

Variables	Non-survivors (n = 42)	Survivors (n = 78)	P-value
Age, years	57.18 ± 11.35	55.34 ± 12.16	0.420
Gender, male/female, n	28/14	57/21	0.529
BMI, kg/m^2	24.19 ± 3.25	24.24 ± 3.31	0.937
APACH II score	26 (22–27)	21 (19–23)	< 0.001
SOFA score	14 (13–18)	10 (9–12)	< 0.001
LIS	3.7 (3.2–4.2)	2.3 (2.0–2.6)	0.001
PaO_2/FiO_2, mmHg	118 ± 43	199 ± 65	< 0.001
CRP, mg/L	136.16 ± 15.08	134.19 ± 16.55	0.523
PCT, ng/mL	1.71 ± 0.43	1.39 ± 0.69	0.007
MiR-150 rel	0.77 ± 0.11	1.18 ± 0.13	< 0.001
IL-1β, pg/mL	183.68 ± 16.64	165.74 ± 16.58	< 0.001
IL-6, pg/mL	79.99 ± 9.09	73.15 ± 7.17	< 0.001
TNF-α, pg/mL	224.17 ± 37.19	191.34 ± 41.99	< 0.001

CRP: C-reactive protein; PCT: procalcitonin.

2.2. Murine model of LPS-induced ALI

Female BALB/c mice at 6 weeks old were obtained from the Experimental Animals Center of Shandong University. All mice were kept in the pathogen-free animal house. Mice (n = 10 per group) were anaesthetized with 2% chloral hydrate (0.2 mL/10 g) and orally intubated into the trachea with a sterile plastic catheter. The ALI model was established by a nasal drip using a lethal dose of LPS (5 mg/kg) in mice for 72 h. In addition, mice injected with the same volume of PBS were used as the control group. The agomir-150 and agomir-NC (RiboBio Co. Ltd., Guangzhou, China) were injected into the mice via tail vein. The expression of miR-150 in the BAL fluid was detected at day 3 following LPS treatment. The lung was then embedded in paraffin, sectioned at 5 μm, and stained with hematoxylin and eosin (HE).

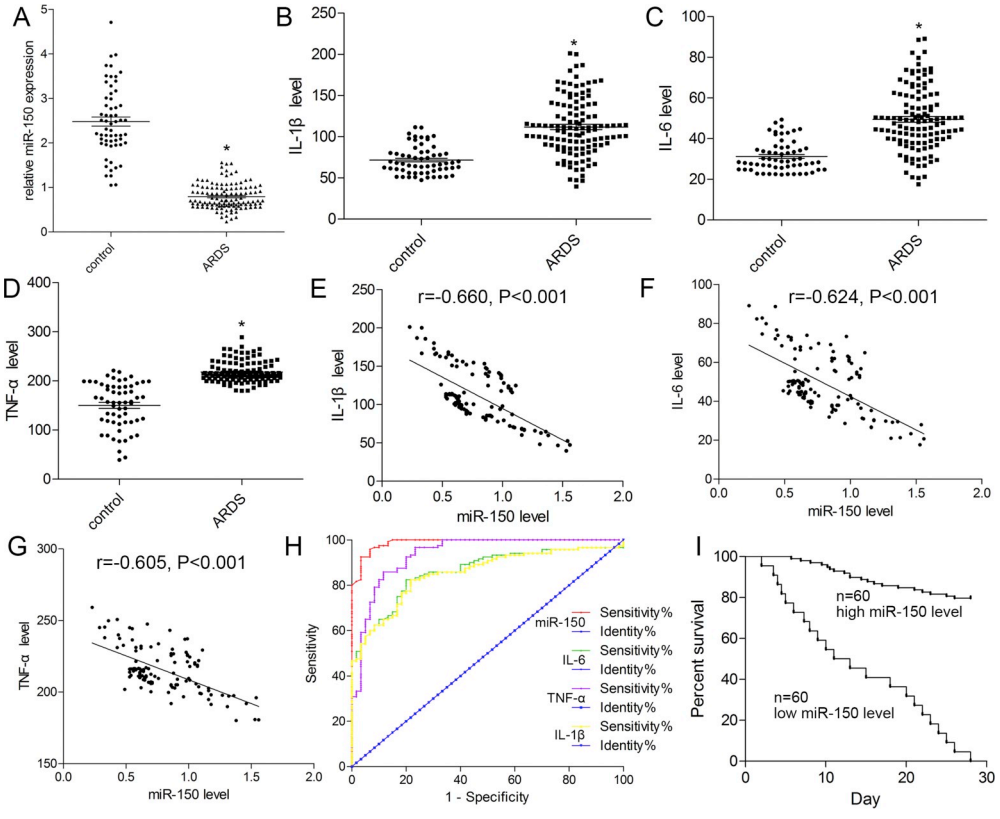

Fig. 1. The expression and significance of miR-150 in patients with ARDS.
(A) Scatter diagram of miR-150 expression between ARDS subjects (n = 120) and healthy controls (n = 60) based on qRT-PCR analysis. Scatter diagram of IL-1β (B), IL-6 (C) and TNF-α (D) expressions between ARDS subjects and healthy controls was shown based on ELISA analysis. The correlations of miR-150 expression with IL-1β (E), IL-6 (F) and TNF-α (G) were determined by bivariate correlation analysis. (H) Diagnostic accuracy was analyzed by ROC curves. (I) Kaplan-Meier analysis was performed for 28-day survival based on the median level of miR-150 expression. Data were expressed as mean ± SD from three independent experiments (n = 3). *P < 0.01, vs. healthy control, using one-way ANOVA test with Tukey's post test.

Table 3
Cox regression analysis of 28-day survival for patients with ARDS.

Variables	Univariate analysis		Multivariate analysis	
	Hazard ratio (95% CI)	P value	Hazard ratio (95% CI)	P value
APACHE II score	1.893 (1.739–4.847)	< 0.001	1.376 (1.063–1.780)	0.015
SOFA score	1.665 (1.266–2.190)	< 0.001	1.472 (1.096–1.975)	0.010
PaO_2/FiO_2	0.622 (0.370–1.047)	0.074	N.A.	N.A.
IL-1β	3.909 (1.367–11.180)	0.011	2.453 (1.356–4.437)	0.003
IL-6	4.526 (1.619–12.654)	0.004	2.947 (1.091–7.959)	0.033
TNF-α	5.108 (1.252–20.838)	0.023	4.171 (1.515–11.483)	0.006
MiR-150	11.15 (3.309–37.572)	< 0.001	9.135 (2.246–37.156)	0.002

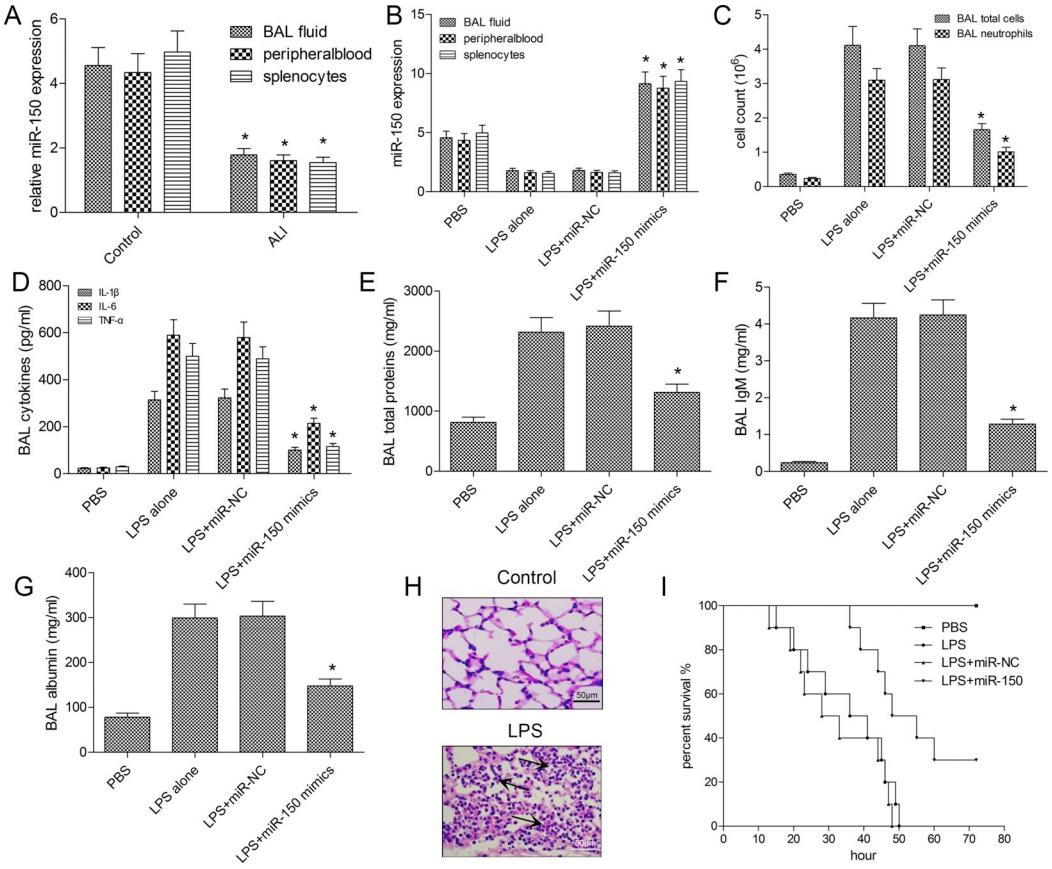

Fig. 2. MiR-150 ameliorates LPS-induced ALI of mice.
(A) miR-150 expression in ALI or control mice was detected by qRT-PCR. (B) The agomir-150 and agomir-NC were injected into the mice via tail vein. The cells in the BAL fluid, peripheral blood, and splenocytes were quantified by hemocytometric counting (C), and the distributions of alveolar macrophages, neutrophils, and lymphocytes were assessed on the basis of their characteristic cell shapes (D). (E) Total protein levels in BAL fluid were assessed by Bradford assay. (F) Total IgM levels were measured by ELISA in BAL fluid. (G) Lung vascular permeability injury induced by LPS was measured by BAL albumin concentration. Albumin levels (mg/mL) were measured by ELISA in the BAL fluid. (H) Representative micrographs of HE-stained lung sections were shown; Lung tissues from PBS-treated mice exhibited normal architectures; Lung tissues from LPS-challenged mice showed severe edema and neutrophil infiltration as indicated with black arrows. Magnification: 400×; Scale bar = 50 μm. (I) Kaplan-Meier survival curves of mice exposed to different groups exhibited a significant improvement in survival compared with mice with LPS alone or other controls, Percentage survival was determined over 72 h. Data were expressed as mean ± SD from three independent experiments (n = 3). *P < 0.01, vs. PBS control or agomir-NC, using one-way ANOVA test with Tukey's post test.

The sections were analyzed microscopically in a blinded fashion for pathologic changes. All procedures were granted by Shandong Provincial Third Hospital Animal Ethical and Welfare Committee (SLSY-A-201801).

2.3. Cell culture

The human pulmonary epithelial cell line A549 was purchased from the Cell Bank of the Chinese Academy of Sciences (Shanghai, China), and then cultured in RPMI-1640 medium (Gibco, Carlsbad, CA, USA) containing 1% glutamine and 10% fetal bovine serum (FBS, Gibco, Carlsbad, CA, USA) in a humidified 37 °C incubator with 5% CO_2.

2.4. Cell transfection

The miR-150 mimics, mimic negative control (miR-NC), small interfering RNA targeting AKT3 (si-AKT3) and control siRNAs (si-control) were purchased from RiboBio Co., Ltd. (Guangzhou, China) and transfected into A549 cells using RFect sRNA Transfection Reagent (Changzhou Biogenerating Biotechnologies Co., Ltd., Jiangsu, China). After 24 h of transfection, the cells were treated with 1000 ng/mL of LPS (Sigma-Aldrich, St. Louis, MO, USA) or dimethyl sulfoxide (DMSO)

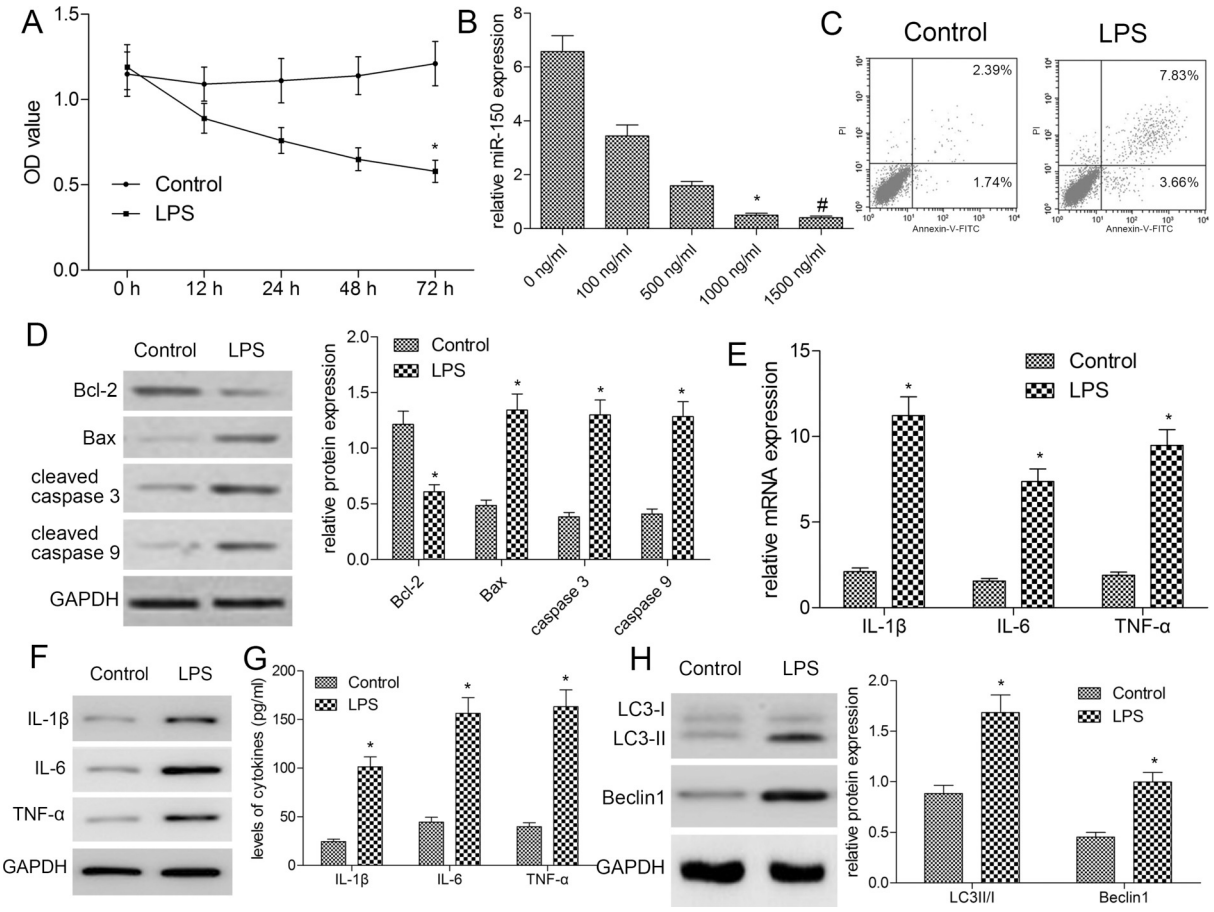

Fig. 3. LPS reduces miR-150 expression and induces A549 cell injury.
Cells were stimulated with 1000 ng/mL of LPS for 72 h. (A) After treatment with 1000 ng/mL of LPS for 72 h, A549 cells were subjected to MTT assay. (B) Concentration curve of miR-150 was detected by qRT-PCR. (C) Apoptosis was evaluated by flow cytometry. (D) The expressions of apoptosis-related proteins were analyzed by Western blot. GAPDH was used as loading control. Left panels are representative western blot bands. Right panels are histogram of quantitative analysis of protein levels. (E) qRT-PCR was used to analyze the expressions of IL-1β, IL-6 and TNF-α mRNAs in A549 cells treated with LPS. (F) The expressions of IL-1β, IL-6 and TNF-α proteins were analyzed by Western blot. (G) The secretion levels of IL-1β, IL-6 and TNF-α were analyzed by ELISA. (H) Cell lysates were subjected to Western blot analysis using antibodies to LC3, Beclin-1, or GAPDH; LC3 was showed in LC3II/I ratio; Beclin-1 was quantitated by densitometry and normalized with GAPDH. Data were expressed as mean ± SD from three independent experiments (n = 3). *P < 0.01, vs. PBS control; #P > 0.05, v.s. 1000 ng/mL LPS, using repeated measures ANOVA test or Student's *t*-test.

(Sigma-Aldrich, St. Louis, MO, USA) for 12, 24 48, and 72 h. It should be noted that the total dose of DMSO should not exceed 0.1% to avoid toxicity.

2.5. qRT-PCR

MiRNA from tissues and cells and total mRNA from cells were respectively extracted using the miRNeasy Mini Kit (Qiagen, Crawley, UK) and the RNAiso Plus Kit (Takara, Dalian, China). The sample RNA was reversely transcribed into cDNA using a reverse transcription kit (TaKaRa, Dalian, China). qPCR was conducted on a CFX96 Real-Time Thermocycler (iCycler, BioRad, Hercules, CA, USA) using SsoAdvanced Universal SYBR Green Supermix (BioRad, Hercules, CA, USA). U6 snRNP were regarded as an internal control. The expression was quantified using the $2-\Delta\Delta Ct$ method. The primer sequences were listed as below:

miR-150:
Forward primer 5′-GCGTCTCCCAACCCTTGTA-3′
Reverse primer 5′-GTGCAGGGTCCGAGGT-3′
U6 SnRNA:
Forward primer 5′-GCGCGTCGTGAAGCGTTC-3′
Reverse primer 5′- GTGCAGGGTCCGAGGT-3′

2.6. Western blot

Tissues or cells were placed in a pre-cooled glass grinder, and a pre-cooled lysate containing PMSF, and phosphatase inhibitors was added and thoroughly ground and lysed. Appropriate amount of 5× protein loading buffer was added to the protein samples. The protein was separated by SDS-PAGE and transferred to PVDF membranes. The membranes were blocked with 5% bovine serum albumin at room temperature for 1 h and then incubated with a specific primary antibody overnight at 4 °C. The corresponding secondary antibodies were incubated for 1 h at room temperature and then the blot was visualized with enhanced chemiluminescence (ECL) method. Data were analyzed with the Molecular Imager (Gel DocTM XR, 170–8170) and the associated software Quantity One-4.6.5 (BioRad, Hercules, CA, USA).

2.7. MTT assay

A total of 1×10^5 cells/mL were plated into 96-well plates, incubated at 37 °C, and cultured overnight. Briefly, 10 μL of MTT (Beijing Solarbio Science & Technology Co., Ltd., Tianjin, China) was added to each well. After 4 h of incubation, the medium was removed and 200 μL of dimethylsulfoxide was added to dissolve the crystal formazan dye. The curve of growth was drawn with the absorbance measured

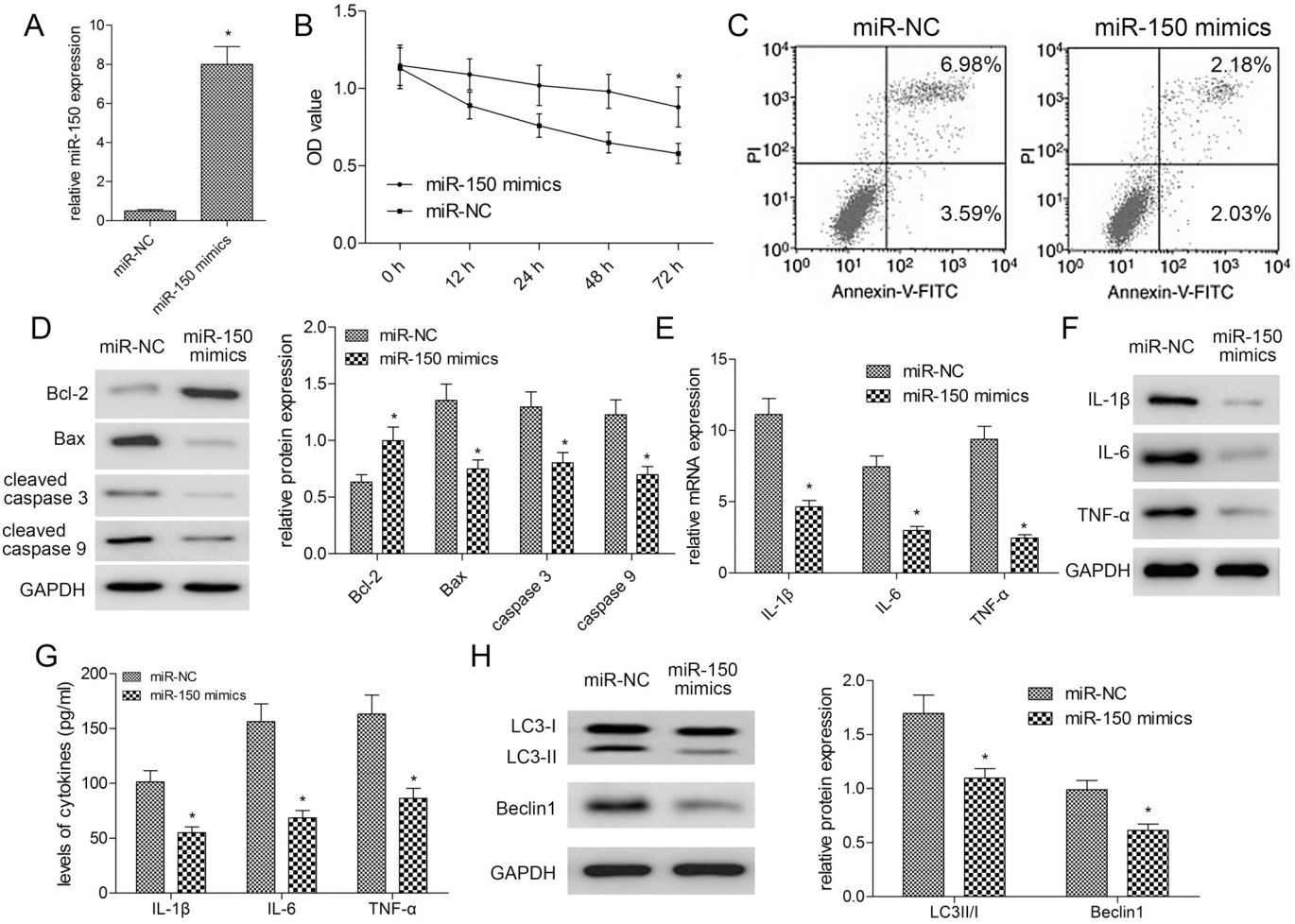

Fig. 4. Over-expression of miR-150 attenuates LPS-induced A549 cell injury. (A) Prior to LPS treatment, A549 cells were transfected with miR-150 mimics or scramble mimics and miR-150 levels were examined after 48 h using qRT-PCR. (B) A549 cells were subjected to MTT assay. (C) Apoptosis was evaluated by flow cytometry. (D) The expressions of apoptosis-related proteins were analyzed by Western blot. GAPDH was shown as loading control. Left panels are representative western blot bands. Right panels are histogram of quantitative analysis of protein levels. (E) Real-time PCR analyzed the expressions of IL-1β, IL-6 and TNF-α mRNAs in A549 cell lines treated with LPS. (F) The expressions of IL-1β, IL-6 and TNF-α proteins were analyzed by Western blot. (G) The secretion levels of IL-1β, IL-6 and TNF-α were analyzed by ELISA. (H) Cell lysates were subjected to Western blot analysis using antibodies to LC3, Beclin-1, or GAPDH; LC3 was showed in LC3II/I ratio; Beclin-1 was quantitated by densitometry and normalized with GAPDH. Data were expressed as mean ± SD from three independent experiments (n = 3). *P < 0.01, vs. miR-NC, using repeated measures ANOVA or Student's t-test.

spectrophotometrically in a microplate reader (BioRad, Hercules, CA, USA) at a wave length of 570 nm.

2.8. Flow cytometry

A549 cells were harvested by trypsinization and were washed with PBS. Cells (1×10^6) from each sample were processed for annexin V-fluorescein isothiocyanate (FITC)/PI apoptosis detection according to the manufacturer's instructions (Becton Dickinson, Franklin Lakes, NJ, USA). All the experiments were repeated at least three times.

2.9. Enzyme-linked immunosorbent assay (ELISA)

Briefly, cell supernatants were collected to detect levels of inflammatory cytokines (IL-1β, IL-6 and TNF-α) using commercial human ELISA Kit (Invitrogen, Carlsbad, CA, USA) according to the manufacturer's protocols. After the substrate reaction, color development was stopped and intensity of color was assayed at 450 nm with reference wave length at 620 nm using a microplate reader (Bio-Rad, Hercules, CA, USA).

2.10. Luciferase reporter assay

The wild-type (WT) 3′-untranslated region (3′-UTR) sequence of AKT3 was amplified using AmpliTaq Gold DNA Polymerase (Applied Biosystems, Foster City, CA, USA). Then the purified WT 3′-UTR was inserted into pmirGLO luciferase plasmid (Biotech, Shanghai) according to the manufacturer's instructions. For mutant (MUT) 3′-UTR, the seed region of the WT 3′-UTR was mutated by AccuPrime Pfx SuperMix (Invitrogen, Carlsbad, USA). The co-transfection of HEK-293 T cells containing miR-150 mimics with WT or MUT 3′-UTR was carried out according to Lipofectamine 2000 (Invitrogen, Carlsbad, CA). After 24 h, the dual-luciferase report assay (Promega, Madison, WI, USA) was done. The renilla luciferase activity was normalized to the corresponding firefly luciferase activity.

2.11. Statistical analysis

Each experiment was repeated at least three times, and all data were presented as mean ± standard deviation (SD). The statistical analyses were evaluated by independent samples *t*-test and analysis of variance (ANOVA) using GraphPad Prism 5 (GraphPad Software, Inc., San Diego, CA, USA). $P \leq 0.05$ was considered as statistically significant.

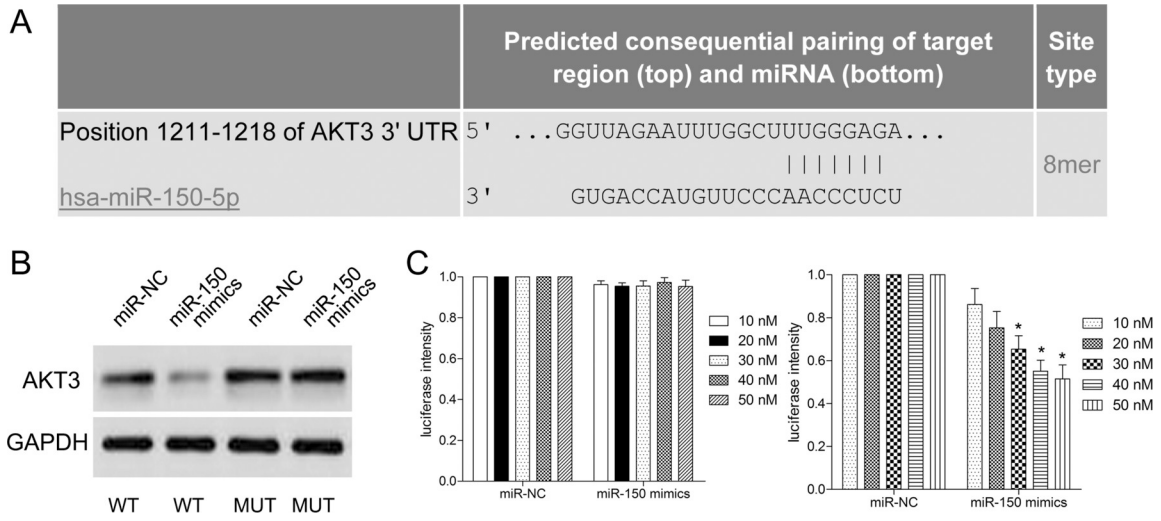

Fig. 5. MiR-150 targets AKT3 directly.
(A) Complementary sequences between miR-150 and AKT3 mRNA 3′-UTR. The pmirGLO Dual-Luciferase miRNA Target Expression Vector was used to construct the WT vector and MUT vector. (B) A549 cells were co-transfected with miR-150 mimics and pcDNA3.1-AKT3 without the 3′-UTR. AKT3 expression was measured by Western blot. (C) HEK-293T cells were transfected with WT AKT3 3′-UTR or mutant AKT3 3′-UTR vector together with miR-150 mimics or miR-NC, then relative activity was measured. Data were expressed as mean ± SD from three independent experiments (n = 3). *P < 0.01, vs. miR-NC, using two-way ANOVA.

3. Results

3.1. MiR-150 level is reduced in the serum of patients with ARDS accompanied by increased inflammatory cytokines

Firstly, we determined that there were no significant differences between ARDS patients and healthy controls in basic clinical variables, such as gender, age, and body mass index (BMI), etc. (Table 1, P > 0.05), and the baseline characteristics were also similar in the survivors and non-survivors (P > 0.05). Then, the blood samples in 120 cases of enrolled patients with ARDS were analyzed to determine the expression level of miR-150 using qRT-PCR assay. We found a significant reduction in the miR-150 level in serum of patients with ARDS compared with the healthy controls (P < 0.01, Fig. 1A). Specially, the expression level of miR-150 in non-survivors was lower than that in survivors (P < 0.01, Table 2). Subsequently, ELISA was conducted to detect the secretion levels of inflammatory cytokines, including IL-1β, IL-6 and TNF-α. We determined that the secretion levels of IL-1β, IL-6 and TNF-α were significantly higher in serum of patients with ARDS compared with healthy controls (P < 0.01, Fig. 1B–D). Particularly, non-survivors had significantly higher secretion levels of IL-1β, IL-6 and TNF-α than those in survivors (P < 0.01; Table 2).

3.2. MiR-150 negatively correlates with disease progression in patients with ARDS

As indicated in Fig. 1E–G, the expression level of miR-150 in serum was inversely associated with the serological levels of IL-1β, IL-6 and TNF-α in patients with ARDS (P < 0.001). In addition, we analyzed the correlations of miR-150 with APACHE II score, SOFA score, lung injury score, and PaO2/FiO2 in ARDS patients. In the included patients with ARDS, the significantly inverse correlations were identified among miR-150 and APACHE II score ($r = -0.778$, P < 0.001), SOFA score ($r = -0.654$, P = 0.001), lung injury score ($r = -0.599$, P < 0.001), respectively. Further, a markedly positive correlation between miR-150 level and PaO2/FiO2 ($r = 0.809$, P < 0.001) was also demonstrated. These data suggested miR-150 may be involved into the progression of ALI/ARDS.

3.3. The diagnosis and prognosis value of miR-150 for patients with ARDS

Receiver operating characteristic (ROC) curves revealed that the optimal cut-off value of miR-150 expression for diagnosis of ARDS was 1.220 (specificity: 96.67%, sensitivity: 92.50%), and the area under the curve (AUC) value of miR-150 was obviously higher (0.989; 95% CI: 0.978–0.999) than that of IL-1β (0.854), IL-6 (0.862) or TNF-α (0.937) (P < 0.001, Fig. 1H). Kaplan-Meier curves for the 28-day survival of patients with ARDS after ICU admission were illustrated in Fig. 1I. Here all subjects were divided into the higher and lower miR-150 group according to median value. Our results validated that ARDS patients with high miR-150 level had a significantly higher 28-day survival rate compared with those with low miR-150 level (P < 0.001). Multivariate Cox proportional hazard regression analysis suggested that in addition to APACHE II scores, SOFA score and cytokines, miR-150 was also an independent risk factor for 28-day survival of ARDS patients (hazard ratio: 9.135, 95% CI: 2.246–37.156; P = 0.002; Table 3).

3.4. MiR-150 ameliorates LPS-induced ALI in vivo

Firstly, we measured the expression level of miR-150 in the BAL fluid of LPS-induced ALI mice at day 3 following LPS treatment. Our results showed that the expression level of miR-150 in BAL fluid was significantly reduced compared with PBS control group (P < 0.01, Fig. 2A). Likewise, miR-150 in peripheral blood and splenocytes was decreased 3 days after treatment in LPS-induced ALI mice (P < 0.01, Fig. 2A). In order to investigate the role of miR-150 in the ALI mice, we injected the miR-150 over-expression vectors into mice, which were further subjected to LPS treatment. It was found that the expression level of miR-150 in the BAL fluid, peripheral blood and splenocytes of mice with miR-150 over-expression was significantly increased by approximately five fold (P < 0.01, Fig. 2B). In addition, enforced expression of miR-150 effectively decreased total inflammatory cell count, especially neutrophil, and the secretion of inflammatory cytokines in the BAL fluid of LPS-induced ALI mice (P < 0.01; Fig. 2C,D). Subsequently, lung permeability of mice was evaluated according to the concentrations of total protein, albumin, and IgM in BAL fluid. As shown in Fig. 2E–G, miR-150 significantly decreased the levels of total protein, albumin and IgM in the BAL fluid from LPS-treated ALI mice (P < 0.05). Consistently, we observed HE stained lung tissue sections, and found that lung tissues from PBS-treated mice showed normal

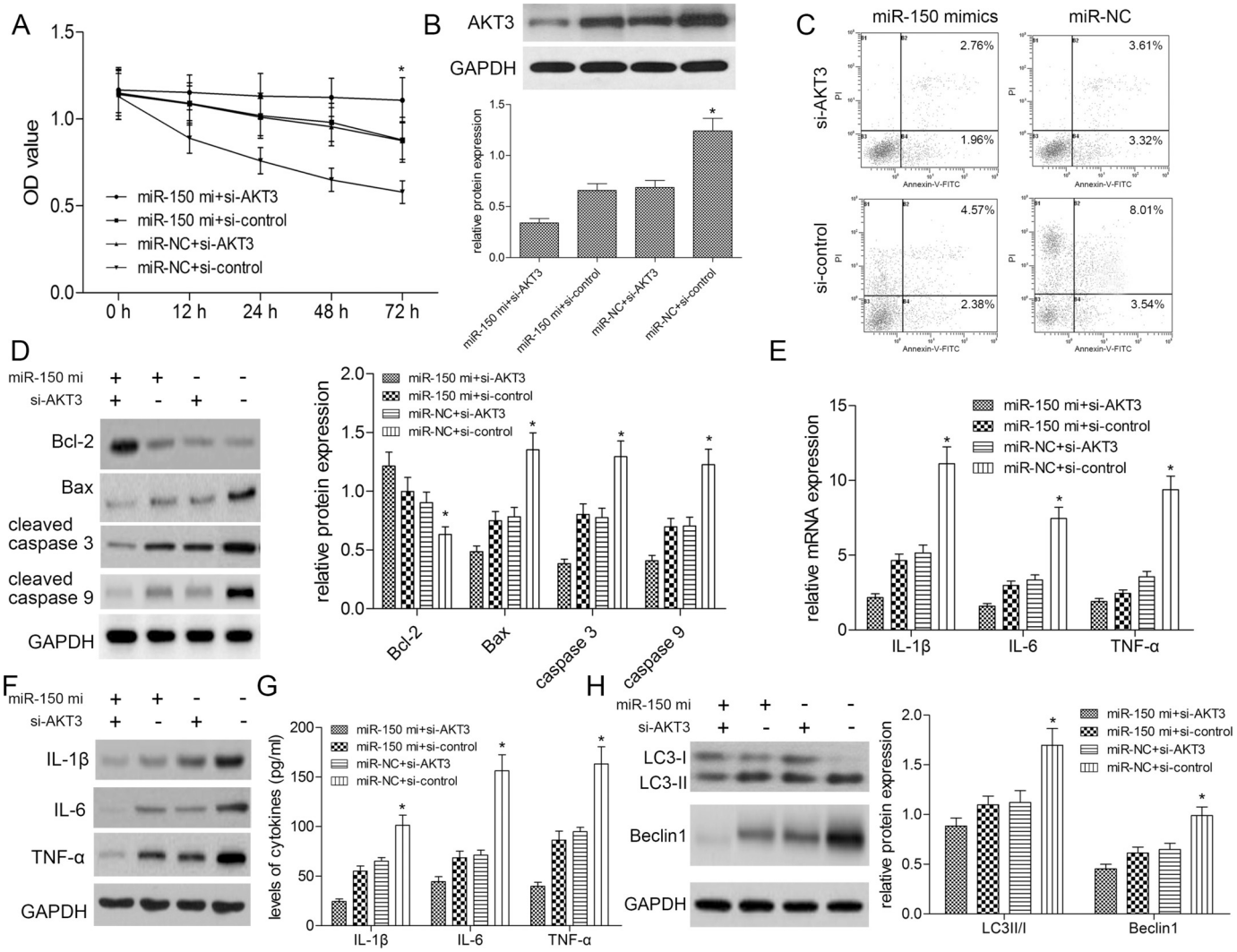

Fig. 6. Silencing of AKT3 enhances protective effects of miR-150 in LPS-induced A549 cell injury.
Prior to LPS treatment (1000 ng/mL of LPS, 72 h), A549 cells were co-transfected with si-AKT3 and miR-150 mimics. (A) A549 cells were subjected to MTT assay. (B) Changes in protein abundance were determined by western blot. (C) Apoptosis was evaluated by flow cytometry. (D) The expressions of apoptosis-related proteins were analyzed by Western blot. GAPDH was shown as loading control. Left panels are representative western blot bands. Right panels are histogram of quantitative analysis of protein levels. (E) Real-time PCR was performed to analyze the expressions of IL-1β, IL-6 and TNF-α mRNAs in A549 cell lines treated with LPS. (F) The expressions of IL-1β, IL-6 and TNF-α protein were analyzed by Western blot. (G) The secretion levels of IL-1β, IL-6 and TNF-α proteins were analyzed by ELISA. (H) Cell lysates were subjected to immunoblot analysis using antibodies to LC3, Beclin-1, or GAPDH; LC3 was showed in LC3II/I ratio; Beclin-1 was quantitated by densitometry and normalized with GAPDH. Data were expressed as mean ± SD from three independent experiments (n = 3). *P < 0.01, vs. miR-NC or si-control, using repeated measures and one-way ANOVA.

architectures, while lung tissues from LPS-treated mice exhibited severe edema and neutrophil infiltration (Fig. 2H). Eventually, we assessed the role of miR-150 in the 72 h survival of ALI mice. As shown in Fig. 2I, on the first day following LPS administration, compared with mice treated with LPS alone, miR-150 obviously prolonged the survival rate of mice with LPS and miR-150 overexpression vector ($P < 0.01$). Further, Kaplan-Meier survival curves from different groups at 72 h demonstrated the statistically significant differences between miR-150 over expression group and three other groups, indicating miR-150 markedly improved the survival rate of ALI mice ($P < 0.01$; Fig. 2I).

3.5. LPS reduced the miR-150 expression and induced A549 cell injury

To figure out the molecular mechanisms of miR-150 in ALI/ARDS, A549 cells were introduced and administrated with 1000 ng/mL of LPS to generate the ALI cell model. We found that LPS markedly repressed cell viability in a time-dependent manner at 72 h after treatment ($P < 0.05$, Fig. 3A). After treatment with different concentrations of LPS for 72 h, the expression level of miR-150 was significantly reduced in a dose-dependent manner ($P < 0.01$, Fig. 3B). When A549 cells were treated with 1000 ng/mL LPS for 72 h, LPS significantly increased apoptosis of A549 cells ($P < 0.001$, Fig. 3C), reduced Bcl-2 level, and elevated Bax, cleaved-caspase-3 and cleaved-caspase-9 levels compared with PBS control ($P < 0.01$, Fig. 3D). Additionally, in comparison with PBS control, LPS obviously increased the secretion levels of IL-1β, IL-6, and TNF-α in A549 cells ($P < 0.001$, Fig. 3E–G) and the expressions of LC3II/I and Beclin1 ($P < 0.05$, Fig. 3H). These data indicated that LPS induced A549 cell injury.

3.6. Over-expression of miR-150 protects A549 cell against LPS-induced injury

To explore the role of miR-150 in LPS-induced A549 cell injury, A549 cells were transfected with miR-150 mimics prior to LPS treatment, then the transfection efficiency was confirmed using qRT-PCR ($P < 0.01$, Fig. 4A). miR-NC was used as control. Over-expression of

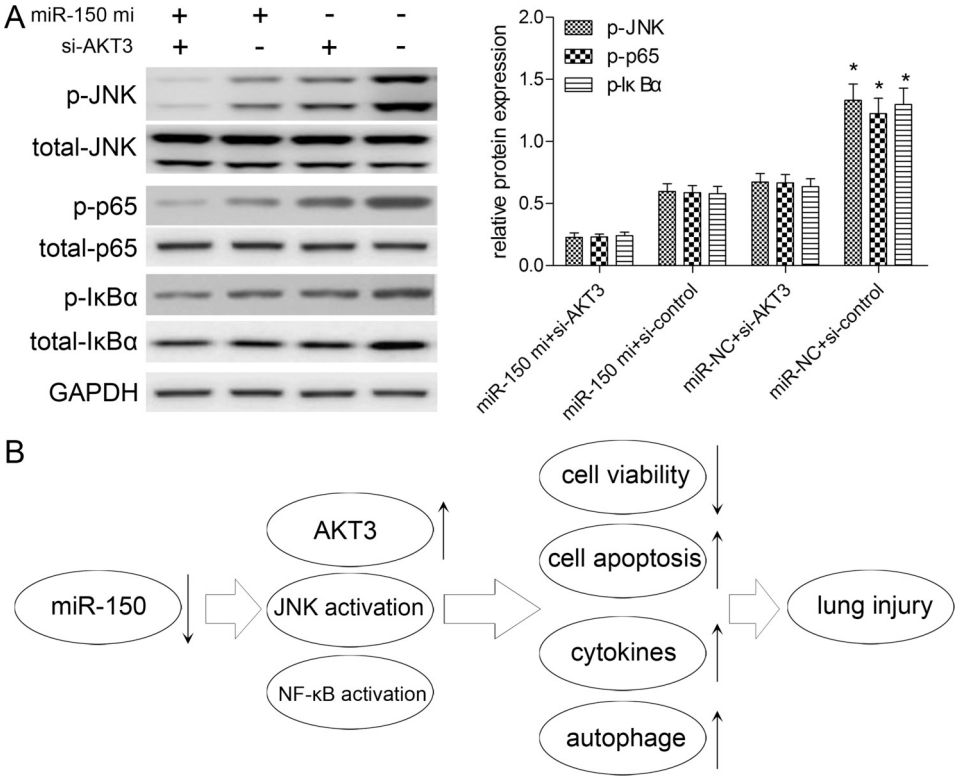

Fig. 7. MiR-150 inhibits JNK and NF-κB pathways.
Prior to LPS stimulation (1000 ng/mL of LPS, 72 h), A549 cells were co-transfected with si-AKT3 and miR-150 mimics. (A) Cell extracts were collected at the indicated times and analyzed by Western blot for the phosphorylation levels of JNK, p65 and IκBα; Total JNK, p65 and IκBα were used as controls. Data were expressed as mean ± SD from three independent experiments (n = 3). *P < 0.01, vs. miR-NC or si-control, using one-way ANOVA. (B) Schematic illustrates that miR-150 targets the expression of AKT3, and inhibits JNK and NF-κB pathways, by which LPS induces A549 cell apoptosis, inflammatory reactions and autopahgy, thereby leading to A549 cell injury.

miR-150 obviously alleviated LPS-inhibited A549 cell viability (P < 0.01, Fig. 4B), inhibited LPS-induced apoptosis (P < 0.01, Fig. 4C), reversed the expression levels of apoptosis-related proteins (Fig. 4D), suppressed the secretion levels of IL-6, IL-1β and TNF-α (P < 0.01, Fig. 4E–G), and decreased the expressions of LC3II/I and Beclin1 (Fig. 4H). These results suggested that LPS-induced A549 cell injury is alleviated by miR-150 over-expression.

3.7. AKT3 is a direct target of miR-150

TargetScan was used to identify the potential target genes of miR-150. Based on putative target sequences at position 1211-1218 of the AKT3 3′-UTR (Fig. 5A), AKT3 was chosen as a potential target of miR-150. Western blot assay demonstrated that the level of AKT3 protein was significantly decreased in A549 cells transfected with miR-150 mimics compared with miR-NC (P < 0.01, Fig. 5B). Subsequently, luciferase reporter assay was further used to confirm the predicted target of miR-150. We demonstrated that miR-150 mimics significantly decreased the relative luciferase activity in HEK-293 T cells co-transfected with AKT3 WT 3′-UTR reporter compared with miR-NC (P < 0.01, Fig. 5C). Nevertheless, the relative luciferase activity in HEK-293 T cells with AKT3 MUT 3′-UTR was not altered (P > 0.05, Fig. 5C). These results validated that AKT3 is indeed a direct target of miR-150.

3.8. Silencing of AKT3 enhances protective effects of miR-150 in LPS-induced A549 cell injury

To elucidate the regulatory relationship between miR-150 and AKT3, we inhibited the AKT3 expression using si-AKT3 transfection in A549 cells. Firstly, the expression of AKT3 protein was markedly reduced in si-AKT3 group compared with si-control (P < 0.01, Fig. 6A). In the presence of LPS, silencing of AKT3 improved A549 cell viability (P < 0.01, Fig. 6B), attenuated cell apoptosis (P < 0.01, Fig. 6C) via increasing the level of Bcl-2 and decreasing the levels of Bax, cleaved-caspase-3 and cleaved-caspase-9 (P < 0.01, Fig. 6D). In addition, silencing of AKT3 inhibited the production of IL-1β, IL-6, and TNF-α (P < 0.01, Fig. 6E–G) and autophagy through reducing the expressions of LC3II/I and Beclin1 (Fig. 6H). Notably, miR-150 mimics together with AKT3 silencing synergically protected A549 cells against LPS-induced cell injury than three other groups (P < 0.01). Our findings suggested that silencing of AKT3 enhances protective effects of miR-150 in LPS-induced A549 cell injury.

3.9. MiR-150 inhibits JNK and NF-κB signalings probably via AKT3

To figure out the relevant signaling pathways involved in the miR-150-regulated A549 cell injury, JNK or NF-κB pathways were investigated due to their putative roles in ARDS. We observed that in comparison with LPS alone, the expression levels of p-JNK, p-p65, and p-IκBα were obviously decreased by miR-150 mimics or si-AKT3 in the presence of LPS (P < 0.01; Fig. 7A). Most importantly, the inhibitory effects of miR-150 mimics alone on the expressions of p-JNK, p-p65, and p-IκBα were greatly aggravated by silencing of AKT3 (P < 0.01; Fig. 7A). Our results inferred that miR-150 inhibited JNK and NF-κB pathways probably through targeting AKT3 pathway.

4. Discussion

In recent years, miR-150 has been identified to be implicated in host response to LPS [9]. Here, we firstly demonstrated that miR-150 was down-regulated, and inversely correlated with the disease severity and 28-day survival in patients with ARDS. Then we successfully established the murine and cellular ALI model, and found miR-150 significantly improved survival of ALI mice, and reduced LPS-induced inflammatory reactions in ALI mice and A549 cells, indicating that miR-150 may be involved in the LPS-induced ALI progression, such as apoptosis and autophagy.

Apoptosis and autophagy regulate cell viability and homeostasis in the progression of ARDS by the apoptosis-/autophagy-related molecules and pathways, including Bcl-2, Bax, cleaved-caspase-3/9, LC3-II/I, and Beclin-1 [10–12]. Generally, apoptosis or autophagy is considered as a kind of protective behavior of normal cells. However, excessive

apoptosis or autophagy in the progression of ARDS can result in injuries of alveolar epithelial cell and vascular endothelial cells [13]. In the present study, miR-150 obviously attenuated LPS-induced apoptosis−/autophagy-related proteins, by which A549 cells survived very well. Together with the report by Zhang [14], our results indicated that miR-150 inhibited LPS-induced autophagy and apoptosis.

Till now, the serine/threonine protein kinase AKT, also known as protein kinase B (PKB), has been demonstrated to participate in the cell apoptosis, DNA damage, and metabolism. Although three members of AKT have a considerable sequence identity in molecular structures, they might play different roles in various diseases [15]. As reported by Chen W [16], luciferase reporter assays in hepatocytes transfected with the Akt1 or Akt2 3′-UTR reporter with or without mutation site identified Akt1 or Akt2 as a direct target of miR-150. In this work, we demonstrated that AKT3 mRNA was a direct target of miR-150. Consistent with our study, AKT3 has been demonstrated to be regulated by miR-29a, miR-338 and miR-145 [17–19]. Further we confirmed that AKT3 knockdown enhanced the protective effect of miR-150 in LPS-mediated A549 cells. At the same time, AKT3 knockdown alone inhibited the inflammatory response, apoptosis and autophagy. Together with these findings, we assumed that miR-150 affects the AKT pathway by targeting AKT3 expression in ALI/ARDS.

Finally, we found that miR-150 over-expression or knockdown of AKT3 inhibited JNK and NF-κB pathways. JNK, a member of mitogen-activated protein kinase family, is required for the production of inflammatory cytokines. Some reports suggested JNK inhibitors can act as a potential therapeutic target in patients with ARDS [20]. NF-κB, a crucial regulator of inflammation, is involved in cell cycle progression, anti-apoptotic process and cytokine secretion [21]. Activation of NF-κB signaling pathway was responsible for inflammatory responses of host response to ALI [22,23]. Together with all findings above, our study indicated that miR-150 plays a pleiotropic role in regulation of AKT, JNK, and NF-κB in the progression of ALI/ARDS. In order to better elucidate the regulatory mechanism of miR-150, the schematic representation is presented in Fig. 7B.

In conclusion, miR-150 protects A549 cells against LPS-induced ALI via directly targeting AKT3. JNK and NF-κB pathways may be directly or indirectly regulated by miR-150/AKT3 pathway in LPS-induced A549 cell injury. Thus, miR-150 can serve as a potential therapeutic target for treating ALI/ARDS.

Author contributions

Pibao Li and Yanbin Chen conceived and supervised the study; Pibao Li, Yanfen Yao, and Yuezhen Ma designed experiments; Pibao Li and Yuezhen Ma performed experiments; Yanbin Chen provided new tools and reagents; Pibao Li and Yanfen Yao analyzed data; Pibao Li and Yanbin Chen wrote the manuscript; Pibao Li and Yanbin Chen made manuscript revisions.

Declaration of Competing Interest

None.

References

[1] M.A. Matthay, R.L. Zemans, G.A. Zimmerman, Y.M. Arabi, J.R. Beitler, A. Mercat, M. Herridge, A.G. Randolph, C.S. Calfee, Acute respiratory distress syndrome, Nat. Rev. Dis. Primers. 5 (1) (2019) 18.

[2] X. Huang, H. Xiu, S. Zhang, G. Zhang, The role of macrophages in the pathogenesis of ALI/ARDS, Mediat. Inflamm. 2018 (2018) 1264913.

[3] J. Zhao, X. Li, M. Zou, J. He, Y. Han, D. Wu, H. Yang, J. Wu, miR-135a inhibition protects A549 cells from LPS-induced apoptosis by targeting Bcl-2, Biochem. Biophys. Res. Commun. 452 (2014) 951–957.

[4] L. He, G.J. Hannon, MicroRNAs: small RNAs with a big role in gene regulation, Nat. Rev. Genet. 5 (7) (2004) 522–531.

[5] I. Slezak-Prochazka, S. Durmus, B. J. Kroesen, Berg. A. den van, MicroRNAs, macrocontrol: regulation of miRNA processing, RNA 16 (6) (2010) 1087–1095.

[6] M.A. Cortez, G.A. Calin, MicroRNA identification in plasma and serum: a new tool to diagnose and monitor diseases, Expert. Opin. Biol. Ther. 9 (6) (2009) 703–711.

[7] C. Vasilescu, S. Rossi, M. Shimizu, S. Tudor, A. Veronese, M. Ferracin, M.S. Nicoloso, E. Barbarotto, M. Popa, O. Stanciulea, M.H. Fernandez, D. Tulbure, C.E. Bueso-Ramos, M. Negrini, G.A. Calin, MicroRNA fingerprints identify miR-150 as a plasma prognostic marker in patients with sepsis, PLoS One 4 (10) (2009) e7405.

[8] C. Roderburg, M. Luedde, D. Vargas Cardenas, M. Vucur, D. Scholten, N. Frey, A. Koch, C. Trautwein, F. Tacke, T. Luedde, Circulating microRNA-150 serum levels predict survival in patients with critical illness and sepsis, PLoS One 8 (1) (2013) e54612.

[9] W.M. Schmidt, A.O. Spiel, B. Jilma, M. Wolzt, M. Muller, In vivo profile of the human leukocyte microRNA response to endotoxemia, Biochem. Biophys. Res. Commun. 380 (3) (2009) 437–441.

[10] I. Dikic, Z. Elazar, Mechanism and medical implications of mammalian autophagy, Nat. Rev. Mol. Cell Biol. 19 (2018) 349–364.

[11] J. Du, X. Zhu, R. Guo, Z. Xu, F.F. Cheng, Q. Liu, F. Yang, L. Guan, Y. Liu, J. Lin, Autophagy induces G0/G1 arrest and apoptosis in menstrual blood-derived endometrial stem cells via GSK3-beta/beta-catenin pathway, Stem Cell Res Ther 9 (2018) 330.

[12] L. Yu, Y. Chen, S.A. Tooze, Autophagy pathway: cellular and molecular mechanisms, Autophagy 14 (2018) 207–215.

[13] M. Zeng, W. Sang, S. Chen, R. Chen, H. Zhang, F. Xue, Z. Li, Y. Liu, Y. Gong, H. Zhang, X. Kong, 4-PBA inhibits LPS-induced inflammation through regulating ER stress and autophagy in acute lung injury models, Toxicol. Lett. 271 (2017) 26–37.

[14] D. Zhang, J. Zhou, L.C. Ye, J. Li, Z. Wu, Y. Li, C. Li, Autophagy maintains the integrity of endothelial barrier in LPS-induced lung injury, J. Cell. Physiol. 233 (2018) 688–698.

[15] E. Gonzalez, T.E. McGraw, The Akt kinases: isoform specificity in metabolism and cancer, Cell Cycle 8 (16) (2009) 2502–2508.

[16] W. Chen, C. Han, J. Zhang, K. Song, Y. Wang, T. Wu, miR-150 deficiency protects against FAS-induced acute liver injury in mice through regulation of AKT, PLoS One 10 (7) (2015) e0132734.

[17] A. Grottke, F. Ewald, T. Lange, D. Norz, C. Herzberger, J. Bach, N. Grabinski, L. Graser, F. Hoppner, B. Nashan, U. Schumacher, M. Jucker, Down regulation of AKT3 increases migration and metastasis in triple negative breast cancer cells by upregulating s100a4, PLoS One 11 (1) (2016) 0146370.

[18] R. Li, J. Liu, Q. Li, G. Chen, X. Yu, miR-29a suppresses growth and metastasis in papillary thyroid carcinoma by targeting AKT3, Tumour Biol. 37 (3) (2016) 3987–3996.

[19] M. Boufraqech, L. Zhang, M. Jain, D. Patel, R. Ellis, Y. Xiong, M. He, N. Nilubol, M.J. Merino, E. Kebebew, miR-145 suppresses thyroid cancer growth and metastasis and targets AKT3, Endocr. Relat. Cancer 21 (4) (2014) 517–531.

[20] X. Huang, G. Kong, Y. Li, W. Zhu, H. Xu, X. Zhang, J. Li, L. Wang, Z. Zhang, Y. Wu, X. Liu, X. Wang, Decitabine and 5-azacitidine both alleviate LPS induced ARDS through anti-inflammatory/antioxidant activity and protection of glycocalyx and inhibition of MAPK pathways in mice, Biomed. Pharmacother. 84 (2016) 447–453.

[21] G. Zhu, X. Xin, Y. Liu, Y. Huang, K. Li, C. Wu, Geraniin attenuates LPS-induced acute lung injury via inhibiting NF-kappaB and activating Nrf2 signaling pathways, Oncotarget 8 (14) (2017) 22835–22841.

[22] L.Y. Jin, C.F. Li, G.F. Zhu, C.T. Wu, J. Wang, S.F. Yan, Effect of siRNA against NF-kappaB on sepsis induced acute lung injury in a mouse model, Mol. Med. Rep. 10 (2) (2014) 631–637.

[23] C. Wu, J. Zhao, G. Zhu, Y. Huang, L. Jin, SiRNA directed against NFkappaB inhibits mononuclear macrophage cells releasing proinflammatory cytokines in vitro, Mol. Med. Rep. 16 (6) (2017) 9060–9066.